Complementarity of gluCEST and ^{1}H-MRS for the study of mouse models of Huntington's disease

Jérémy Pépin, Lucie de Longprez, Fabrice Trovero, Emmanuel Brouillet, Julien Valette, Julien Flament

Title

Complementarity of gluCEST and ^{1}H-MRS for the study of mouse models of Huntington's disease

Authors

Jérémy Pépin[a,b], Lucie de Longprez[a,b], Fabrice Trovero[c], Emmanuel Brouillet[a,b], Julien Valette[a,b], Julien Flament[a,b]

Affiliations

[a]Commissariat à l'Energie Atomique (CEA), Direction de la Recherche Fondamentale (DRF), Institut de biologie François Jacob, Molecular Imaging Research Center (MIRCen), Université Paris-Saclay, F-92260 Fontenay-aux-Roses, France

[b]Centre National de la Recherche Scientifique (CNRS), Université Paris-Sud, Université Paris-Saclay, UMR 9199, Neurodegenerative Diseases Laboratory, F-92260 Fontenay-aux-Roses, France

[c]Key-Obs SAS, 13 avenue Buffon, F-45100 Orléans, France

Corresponding author

Dr. Julien Flament

MIRCen, CEA, 18 route du Panorama - BP n° 6

92265 - Fontenay-aux-Roses Cedex, France

julien.flament@cea.fr

Grants and sponsors

"HDeNERGY" project (ANR-14-CE15-0007-01)

"epiHD" project (ANR-17-CE12-0027)

"TreatPolyQ" project (ANR-17-RAR3-0008-01)

The 11.7T MRI scanner was funded by a grant from NeurATRIS "Investissements d'Avenir" (ANR-11-INBS-0011)

Number of figures: 5 and **tables:** 0

Number of References: 40

Words count for: Abstract: 277 **; Text:** 3461

Keywords

GluCEST

^{1}H-MRS

Huntington's disease

Glutamate

Mouse model

Neurodegenerative disease

Abstract

Identification of relevant biomarkers is fundamental to understand biological processes of neurodegenerative diseases and to evaluate therapeutic efficacy. Atrophy of brain structures has been proposed as a biomarker but it provides little information about biochemical events related to the disease. Here, we propose to identify early and relevant biomarkers by combining biological specificity provided by ^{1}H-MRS and high spatial resolution offered by gluCEST imaging. For that, two different genetic mouse models of Huntington's disease, the Ki140CAG model characterized by a slow progression of the disease and the R6/1 model, which mimics juvenile form of HD, were used. Animals were scanned at 11.7T using a protocol combining ^{1}H-MRS and gluCEST imaging. We measured significant decrease of N-acetyl-aspartate levels, a metabolite mainly located in the neuronal compartment, in HD animals and the decrease seemed correlated with disease severity. In addition, variations of tNAA levels were correlated with striatal volumes in both models. Significant variations of glutamate levels were also observed in Ki140CAG but not in R6/1 mice. Thanks to its high resolution, gluCEST provided complementary insights, and we highlighted alterations in small brain regions such as the corpus callosum in Ki140CAG mice whereas glutamate level was unchanged in the whole brain of R6/1 mice. In this study, we showed that ^{1}H-MRS can provide key information about biological processes occurring in vivo but was limited by the spatial resolution. On the other hand, gluCEST may finely point to alterations in unexpected brain regions, but it can also be blind to disease process when glutamate levels are preserved. This highlights in a practical context the complementarity of both methods to study animal models of neurodegenerative diseases and to identify relevant biomarkers.

Introduction

Neurodegenerative diseases are characterized by a slow degeneration of the neuronal structure, leading to cognitive, psychiatric and motor symptoms like in Huntington's disease (HD). Because of population aging and increase of life expectancy, their prevalence is increasing constantly and will become a major public health issue in the coming years.

These disorders are very complex and can exhibit various hallmarks at molecular or cellular levels such as oxidative stress, neuroinflammation, transcriptional and epigenetic deregulation, mitochondrial impairments or defects in Ca^{2+} homeostasis (1, 2). In most cases, neurodegenerative diseases are of unknown origin. However, some diseases such as HD are mostly inherited and can therefore be easily diagnosed. Neuroimaging of these genetic diseases can provide relevant biomarkers, for instance atrophy of the striatum measured in HD patients (3, 4), which are of interest to characterize disease progression. However, little is known about biological mechanisms underlying degenerative processes. In spite of tremendous efforts made, there is currently no treatment to cure neurodegenerative diseases or to slow down their progression. A key point towards development of innovative therapeutic approaches is the identification of relevant biomarkers to allow early detection and accurate monitoring of disease progression. Moreover, such biomarkers would be extremely informative to evaluate therapeutic response of potential treatments.

In addition to cognitive and/or motor tests, anatomical imaging is one of the most robust criteria to characterize disease progression. For instance, MRI can be used to accurately measure macroscopic alterations of brain structures. Although very informative as they can be reliable markers of disease progression (3-5), morphological changes are likely a long-term reflect of biological events that occurred several years before brain cell degeneration. Besides, structure alterations provide poor information about cellular and biochemical events occurring in the disease (6).

Thanks to its intrinsic ability to distinguish specific proton resonances, in vivo MRS can provide rich and valuable insights into biological processes in healthy or pathological conditions. Among all metabolites, glutamate (Glu) and N-acetylaspartate (NAA) are relevant in the context of neurodegenerative diseases as they are considered as good neuronal markers (7-9). In addition, myo-inositol (Ins) and glutamine (Gln) are potential markers of glial proliferation (10). Numerous studies have already demonstrated the interest of ^{1}H-MRS to detect early onset of neurodegenerative disorders (11-13). Unfortunately, ^{1}H-MRS has very low sensitivity and hence limited spatial resolution.

Therefore, bridging the gap between biological information provided by ^{1}H-MRS and spatial information provided by anatomical MRI remains a key challenge. Recently, CEST (Chemical Exchange Saturation Transfer) has been proposed to image dilute molecules in vivo with a good spatial resolution (14, 15). The potential of CEST imaging, and particularly CEST imaging of glutamate (gluCEST) has already been demonstrated in human (16, 17) and animal models of neurodegenerative diseases (18-20). ^{1}H-MRS and gluCEST are promising methods to identify in vivo biomarkers. While both methods are usually used for cross validation, to date no preclinical study has actually demonstrated specific interests of each method. In addition, the wide heterogeneity of animal models for a same pathology can render difficult the choice of the appropriate method for monitoring disease progression or evaluating treatment efficacy. In this study,

we used two mouse models of HD (Ki140CAG and R6/1) exhibiting different hallmarks of the pathology (21) in order to highlight the complementarity of ^{1}H-MRS and gluCEST for the study of neurodegenerative diseases.

Materials and methods

Two mouse models of HD

The first model was a knock-in model expressing chimeric mouse/human exon 1 containing 140 CAG repeats inserted in the murine huntingtin (*Htt*) gene (Ki140CAG) (22). It is characterized by slow progression of motor and cognitive symptoms as well as cellular and molecular abnormalities leading to neurodegeneration (22). Twelve-month old mice were divided in 3 groups: heterozygous (Ki140-Hetero., n = 5), homozygous (Ki140-Homo., n = 5) for the *Htt* gene and wild type littermate controls (Ki140-WT, n = 5). The Ki140CAG mice dataset is the same as the one already published in a previous study (19). The second model was a transgenic model expressing mouse/human exon 1 containing 115 CAG repeats in the human huntingtin (*HTT*) gene (R6/1) (23). Mice exhibit motor deficits and striatal atrophy as early as 4 months and decline in motor performances correlates with the appearance of huntingtin aggregates in striatal neurons (24). The disease progression is more aggressive than in the Ki140CAG model and mimics the juvenile form of HD. Seven-month old mice were divided in two groups: heterozygous for *Htt* gene (R6/1-Hetero., n = 4) and wild type littermate controls (R6/1-WT, n = 3).

Animal studies were conducted according to the French regulation (EU Directive 2010/63/EU — French Act Rural Code R 214-87 to 131) and procedures received approval from the ethical committee (APAFIS#770). Mice were anesthetized using around 1.5% isoflurane in a 1:1 gas mixture of air/O_2. Mice temperature was monitored and maintained at 37 °C and respiratory rate was continuously monitored using PC SAM software (SA Instruments, USA).

^{1}H-MRS and gluCEST data acquisition

Acquisitions were performed on a horizontal 11.7 T scanner (Bruker, Ettlingen, Germany). ^{1}H-MRS spectra were acquired using a quadrature cryoprobe (Bruker, Ettlingen, Germany) with a LASER (Localization by Adiabatic Selective Refocusing) sequence (echo time (TE)/repetition time (TR) = 20/5000 ms) combined with VAPOR water suppression in a voxel of 8 µL (2 x 2 x 2 mm^3) located in the left striatum. Spectra were acquired using 128 repetitions in 10 min. Metabolite concentrations were quantified using LCModel (25), including the macromolecule (MM) spectrum of a control mouse that was determined by metabolite nulling and included in LCModel's basis-set. The following metabolites were reliably quantified (Cramér-Rao lower bound ≤ 5%): total choline (tCho), total creatine (tCr), glutamate (Glu), glutamine (Gln), myo-inositol (Ins), total N-acetyl-aspartate + N-acetyl-aspartyl-glutamate (tNAA) and taurine (Tau). Metabolite concentrations were normalized with respect to 8 mM tCr.

GluCEST data were acquired with a volume coil for radiofrequency transmission and a quadrature surface coil for reception (Bruker, Ettlingen, Germany). The sequence consisted in a 2D fast spin-echo preceded by

a frequency-selective continuous wave saturation pulse (150 × 150 μm^2 in-plane resolution, field of view = 19.2 x 19.2 mm^2, matrix size = 128 x 128, 0.6 mm slice thickness, 3 contiguous slices, TR = 5000 ms, 10 echoes and effective TE = 30 ms). The saturation module was composed by 10 broad pulses of 100 ms, with 20-μs inter-delay (T_{sat} = 1 s) and amplitude B_1 = 5 μT. The frequency of the saturation pulse Δω was applied within a range from −5 ppm to 5 ppm with a step of 0.5 ppm. B_0 correction was performed using WASSR method (26). The specific glutamate contribution was isolated using Asymmetrical Magnetization Transfer Ratio (MTRasym) centered at ±3 ppm. Variation maps of gluCEST contrast between WT littermates and HD mice were calculated in each Region of Interest (ROI) as already described (19): Variation = 100 x (MTRasym(WT) - MTRasym(HD)) / MTRasym(WT). ROI segmentation was performed manually by a single operator with help of the Allen mouse brain atlas using the reference CEST image acquired without saturation. T_2-weighted images acquired with Multi Slices Multi Echoes (MSME) sequence (TE/TR = 5/2500 ms, 17 echoes, effective TE = 45 ms, in-plane resolution = 70 × 70 μm^2, 25 slices with thickness = 300 μm) were used for striatal volume measurements. For comparison of gluCEST and ^{1}H-MRS data, we calculated the mean gluCEST contrast in a 2 x 2 mm² square ROI located in the left striatum in three contiguous slices. The volume of the ROI used for gluCEST analysis was 2 x 2 x 1.8 mm^3, which was comparable to the spectroscopic voxel.

Results

Striatal volume

We observed a significant 20.9% decrease (p = 0.002) of striatal volume in Ki140CAG homozygous mice as compared to WT littermates (Fig.1). A milder atrophy was observed in Ki140CAG heterozygous mice but this did not reach statistical significance (-10.1%, p = 0.11, Fig.1). A marked striatal atrophy was measured in R6/1 mice as compared to their respective WT littermates (-25.7%, p = 0.00002, Fig.1). Noticeably, we observed a larger striatal volume in control R6/1 mice (22.8 ± 0.9 mm^3) than in control Ki140CAG mice (18.7 ± 0.7 mm^3), possibly due to the difference in age (7-month and 12-month old for R6/1 and Ki140CAG mice respectively) and/or mouse strains.

^{1}H-MRS

We observed a significant decrease of tNAA in the left striatum in both models (-17.4% and -24.3% in Ki140-Hetero and Ki140-Homo respectively and -36.4% in R6/1-Hetero, Fig.2) as compared to their respective WT littermates. Taurine exhibited a significant 25.9% and 33.3% decrease in heterozygous and homozygous Ki140CAG mice respectively. A significant 13.0% decrease of Glu was observed in heterozygous Ki140CAG mice. Glu concentration was also decreased in homozygous Ki140CAG mice (-14.9%) even though the variation was not significant (p = 0.06). Finally, significant variations of Gln (+27.4%) and tCho (−21.7%) were measured in homozygous Ki140CAG mice.

Surprisingly, tNAA was the only metabolite showing significant variation in R6/1 mice (Fig.2). In order to study potential correlations between biological information provided by ^{1}H-MRS and anatomical information,

the concentration of tNAA measured in the left striatum was plotted as a function of the striatal volume V_{striat} for each mouse cohort (Fig.3). We observed a proportional relationship between the tNAA concentration and the striatal volume for both models ([tNAA] = 0.31 V_{striat} + 1.55 (R^2 = 0.97) for Ki140CAG mice and [tNAA] = 0.37 V_{striat} – 2.15 for R6/1 mice). No other metabolite exhibited similar dependency to the striatal volume.

GluCEST

An example of gluCEST images acquired in one mouse of each cohort is shown in Fig.4.a. As already described, Ki140CAG mice exhibited decreased levels of gluCEST contrast across the whole brain with a stronger effect observed in the homozygous mouse (Fig.4.a, top panel). This “gene-dose” effect was confirmed by the mean MTRasym curves calculated for each group of mice in a volume comparable to the voxel used in ^{1}H-MRS mostly located into the left striatum (Fig.4.c). As illustrated by individual examples (Fig.4.a, bottom panel) and mean MTRasym curves (Fig.4.e), no variation of gluCEST contrast was measured in R6/1 mice as compared to their respective WT littermates.

Eight ROIs were drawn manually in the brain of each mice (Fig.5, top left panel) and mean gluCEST contrast was calculated in each ROI for each mice group. Variations of gluCEST contrast between WT and HD mice were calculated as described previously (19). Ki140-Homo mice exhibited significant decreases of gluCEST contrast in the striatum and the piriform cortex (Fig.5, bottom right). On the contrary, these structures did not reach statistical significance in Ki140-Hetero mice (Fig.5, bottom left), confirming a “gene-dose” effect in this mouse model. The most striking result was the strong and significant decrease of gluCEST contrast in the corpus callosum in both heterozygous and homozygous Ki140CAG mice (-21.8% and -28.4% respectively) as mentioned in our previous work (19). In contrast, no variation of gluCEST contrast was found in R6/1 mice in any brain region (Fig.5, top right).

Discussion

Animal models are valuable tools for neuroscientists as they offer the possibility to specifically focus on one or several aspects of the pathology. Numerous studies have demonstrated the interest of animal models to study common hallmarks of HD pathogenesis like striatum atrophy, presence of huntingtin aggregates, motor and behavioral symptoms or modification of metabolic profiles (19, 27-29). However, these studies also highlighted the wide heterogeneity of animal models and variety of relevant biomarkers for a same pathology. Thus, the choice of the appropriate method to study one particular model is not straightforward. In this study, we used two mouse models of HD known to mimic different stages of the pathology in order to evaluate the complementarity of ^{1}H-MRS and gluCEST to identify relevant in vivo biomarkers of HD. The Ki140CAG model is considered as a slowly progressive model reproducing the progression of the disease in HD patients (30) whereas the transgenic R6/1 model is considered as a severe HD model that mimics juvenile onset of HD (23).

Cell specific alterations observed by MRS

^{1}H-MRS has unique ability to measure intracellular metabolite concentrations, providing plenty of information about biological alterations. In particular, as tNAA is mostly located in the neuronal compartment, it is considered has a marker of neuronal integrity and function (7-9). In these models, tNAA levels were systematically lower in HD animals. Interestingly, the decrease seemed correlated with disease severity as tNAA decreases measured in Ki140CAG mice (-17.4% and -24.3% in Ki140-Hetero and Ki140-Homo respectively, Fig.2) were smaller than that measured in the more severe R6/1 model (-36.4%, Fig.2). In addition, variations of tNAA levels were correlated with striatal volumes and proportionality coefficients were comparable in both models (Fig.3). Interestingly, R6/1 and Ki140CAG mice exhibited decrease of tNAA level even in absence of actual neuronal loss measured at 7 months (31, 32) and 12 months (22) respectively. The decrease of striatal volume can be explained by neurons shrinkage, reduced cell complexity and dendritic arborization (27). The reduction in tNAA levels in mouse models is coincident with decreased levels of mRNA and proteins that are considered as molecular markers of the striatum, i.e. preferentially expressed in striatal medium sized spiny neurons (33, 34). For example, reduced levels of the mRNA and/or protein of striatal markers such as Dopamine and 3′,5′-Cyclic Adenosine Monophosphate-Regulated Neuronal Phosphoprotein (known as DARPP-32), phosphodiesterase 10 (PDE10) or the recently studied doublecortin-like kinase 3 (DCLK3) have been observed in Ki140CAG and R6/1 mice (33-36). The levels of these markers have also been found to be reduced in post-mortem samples in HD patients (36). In spite of the absence of neuronal loss at 12 months, both models showed behavioral phenotypes (19, 22, 31, 32). Thus, such results are in line with the idea that tNAA level is related to neuronal cell suffering and could be a potential marker of neuronal functions alteration (37). It is interesting to note that basal levels of tNAA and striatal volumes were not comparable between the two models, especially between WT mice of each cohort (Fig.3). However, such discrepancies can be explained by the difference in age of the cohorts as well as the difference in genetic background used to generate the models and breed the colonies. Moreover, breeding conditions and genetic drift can lead to different phenotypes of mouse colonies bred in different laboratories (24). Consequently, it is difficult to compare brain metabolites levels and structures volumes between control animals of each cohort.

Glutamate is one of the main neurotransmitters into the brain. Even if Glu released in the synaptic cleft is taken up by astrocytes, most of Glu is located in the neuronal compartment. Thus, Glu is often considered as a potential neuronal marker (7-9). However, in this study, no correlation between striatal volume and Glu level was found in R6/1 mice (data not shown). Comparable results have already been reported in R6/2 mice, a similar but more aggressive HD model than R6/1, where Glu levels measured in the cortex and the striatum of R6/2 were stable as compared to WT littermates, while cortical and striatal volumes were decreased by ~20% and ~32% respectively, and tNAA levels were decreased by ~33% and ~29% respectively (29) at 15 weeks. In Ki140CAG mice, we observed a decrease of Glu levels but no neuronal loss was observed on histological sections using NeuN staining, a neuronal maker (19). However, the decrease in Glu levels was associated with increase in Gln in Ki140CAG mice whereas they were stable in R6/1 mice. Interestingly, Glu could be used as a potential marker of reorganization of energy metabolism and metabolic fluxes. Indeed, such results could indicate an imbalance in glutamate-glutamine cycle in

Ki140CAG mice which is important for energy homeostasis (38). In addition, Glu can also be implicated in energy production through its equilibrium with alpha-ketoglutarate, an intermediate of the Krebs cycle. One can hypothesize that dynamic adaptations of metabolic fluxes may take place during the animal lifespan in order to counterbalance disturbance of homeostasis and energy production due to mutant huntingtin (39). One can assume that such compensatory mechanisms would be more efficient in slowly progressive models than in severe forms where the aggravation of the alterations of brain cells are probably faster and might not be counterbalanced. The exact mechanisms underlying the differences between R6/1 and KI140CAG are not known but likely results from the differences in terms of the proper genetic modifications found in the two models: while KI140CAG express one copy (heterozygous) of the whole mouse *Htt* gene with a part of the exon 1 of mutant human *HTT* gene under the murine Htt promoter, the R6/1 model express 4 to 5 copies of only the exon 1 of human *HTT*, leading more rapidly to neurotoxicity (21).

Complementarity of ^{1}H-MRS and gluCEST imaging

While ^{1}H-MRS can provide rich and specific information about biological processes in vivo, it suffers from a lack of spatial resolution. It requires large voxels which can be problematic for studying small or heterogeneous structures. Moreover, voxel positioning is based on a priori knowledge about the pathology. Consequently, potential alterations in unsuspected structures can be missed. On the contrary, gluCEST imaging can provide high resolution metabolic imaging where partial volume effect and surrounding structures contamination are minimized. Results already published (19) obtained in the Ki140CAG model demonstrated this advantage by highlighting strong alterations of glutamate levels in the corpus callosum of HD mice. Interestingly, variation of gluCEST contrast was even more pronounced in homozygous mice than in heterozygous, confirming a “gene-dose” effect in this model (Fig.5). Such measurements would have been hardly achievable using ^{1}H-MRS due to the important contamination from surrounding structures.

On the other hand, the gluCEST variation map acquired in R6/1 mice was very stable, the strongest variation being -2.4% (but not significant, $p = 0.746$) measured in the left somatosensory cortex. Such variations are below the detection threshold estimated at ±4% in our previous study (19). Nonetheless, the stability of gluCEST map in R6/1 mice was very informative as it suggested that no brain region exhibited alteration of Glu levels in this model. Note that some individual examples of gluCEST maps exhibited a slight heterogeneity of gluCEST contrast, especially in the cortical region (Fig.4.a). However, we did not observe a systematic bias over all animals and no difference was observed between left and right hemispheres at the scale of mice cohorts (19), ruling out a possible bias due to mouse positioning or coil inhomogeneity. Further investigations would be necessary to elucidate the origin of such heterogeneity at the individual scale.

Finally, we compared Glu concentrations measured by ^{1}H-MRS in the left striatum (Fig.2.b) with gluCEST contrasts measured in a comparable volume in Ki140CAG-WT and R6/1-WT (Fig.4.c and .e respectively). Interestingly, R6/1-WT mice exhibited a gluCEST contrast that was 19.6% lower than that of Ki140CAG-WT mice (MTRasym = 11.9%, Fig.4.e and MTRasym = 14.8%, Fig.4.c, respectively). This was consistent with the 20.0% difference of Glu concentration measured by ^{1}H-MRS between wild type Ki140CAG and wild type R6/1 (6.44 mM and 8.05 mM respectively, Fig.2.b). In addition, comparison of Z-spectra upfield from the

water resonance acquired in Ki140-CAG (Fig.4.b) and R6/1 mice (Fig.4.d) showed very small differences. This means that magnetization transfer between water and non-exchangeable protons was unaltered in HD animals and the asymmetrical approach used to characterize gluCEST contrast was valid. While other contributions to the CEST contrast by non-specific magnetization transfer effects or by endogenous metabolites such as GABA or taurine cannot be excluded, such observations seems to indicate that gluCEST contrast is dominated by Glu concentration, as already described for comparable saturation parameters (20, 40).

Conclusion

By combining ^{1}H-MRS and gluCEST, we have shown striking differences between these two mouse models. The decrease of tNAA levels measured in R6/1 mice suggested an alteration of the neuronal compartment but the stability of other metabolites argued in favor of integrity of the astrocytic compartment and energy metabolism. In Ki140CAG mice, a slowly progressive model, modifications of several metabolite levels could reflect homeostatic changes to compensate deficits that occurred early in mouse's life. Moreover, gluCEST was able to evidence alterations in unexpected brain regions such as the corpus callosum. However, this method may also be blind to disease process in certain situations where glutamate levels are preserved. This highlights the complementarity of both methods to identify relevant biomarkers, especially in the context of HD. Acquisition of ^{1}H-MRS and gluCEST data within a same protocol could provide various readouts to monitor disease progression or treatment efficacy and improve the use of animal models for the study of a large spectrum of neurodegenerative diseases.

Acknowledgments

This work was supported by two grants from Agence Nationale pour la Recherche ("HDeNERGY" project ANR-14-CE15-0007-01 and "epiHD" project ANR-17-CE12-0027) and one grant from the ERA-Net for Research Programs on Rare Diseases ("TreatPolyQ" project ANR-17-RAR3-0008-01). The 11.7T MRI scanner was funded by a grant from NeurATRIS: A Translational Research Infrastructure for Biotherapies in Neurosciences ("Investissements d'Avenir", ANR-11-INBS-0011).

Figures and legends

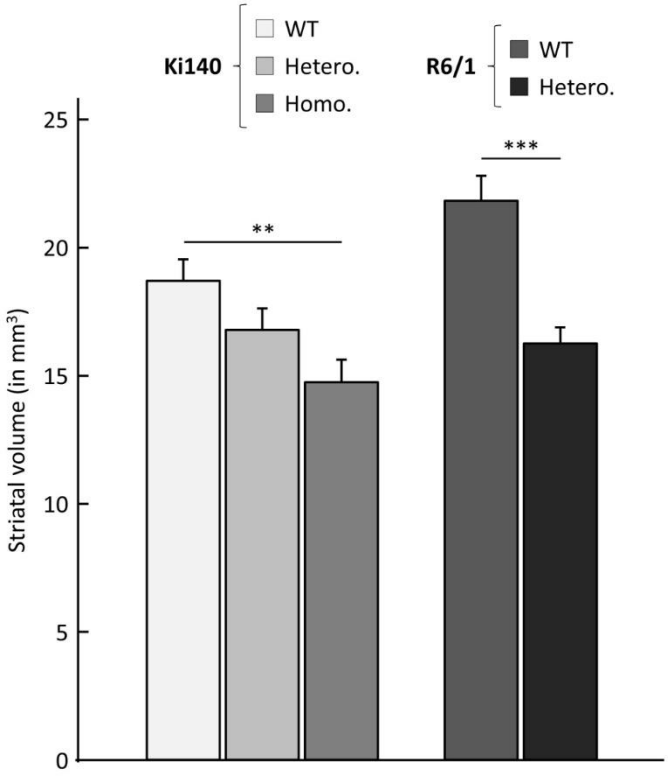

Figure 1: Striatal atrophy measured by MRI in Ki140CAG and R6/1 mice. Striatum volume was measured in Ki140-WT (n = 5), Ki140-Hetero. (n = 5), Ki140-Homo. (n = 5), R6/1-WT (n = 3) and R6/1-Hetero (n = 4) mice. Data are presented as mean ± SEM. Statistical analysis was performed by Student's t-test for R6/1 mice and by one-way ANOVA (significant threshold set to 0.05) with Fisher's LSD *post hoc* test for Ki140CAG mice (*$p < 0.05$; **$p < 0.01$; ***$p < 0.001$).

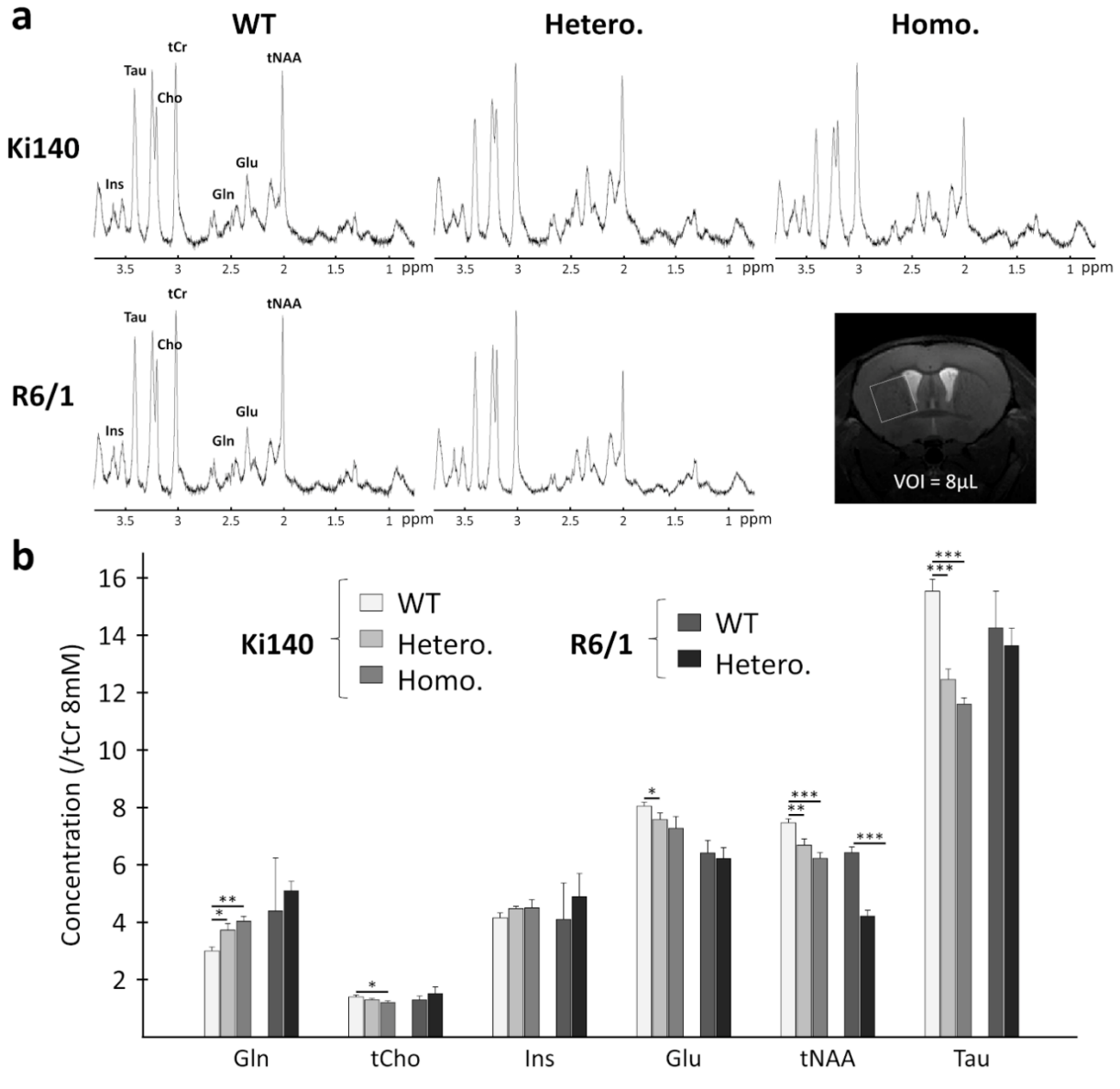

Figure 2: ^{1}H-MRS of Ki140CAG and R6/1 mice. a) Examples of ^{1}H-spectrum acquired in a voxel of 8 µL located in the left striatum (see inset) of one mouse from each group of Ki140CAG mice (top panel) and R6/1 mice (bottom panel). The following metabolites, total choline (*tCho*), total creatine (*tCr*), glutamate (*Glu*), glutamine (*Gln*), myo-inositol (*Ins*), total N-acetyl-aspartate + N-acetyl-aspartyl-glutamate (*tNAA*) and taurine (*Tau*), were reliably quantified (CRLB < 5%). **b)** Metabolic profiles measured by ^{1}H-MRS in Ki140CAG and R6/1 mice. Concentration of metabolites normalized with respect to 8 mM tCr were measured in left striatum of Ki140-WT (n = 5), Ki140-Hetero. (n = 5), Ki140-Homo. (n = 5), R6/1-WT (n = 3) and R6/1-Hetero (n = 4) mice. Data are presented as mean ± SEM. Statistical analysis was performed by Student's t-test for R6/1 mice and by one-way ANOVA (significant threshold set to 0.05) with Fisher's LSD *post hoc* test for Ki140CAG mice (*p < 0.05; **p < 0.01; ***p < 0.001).

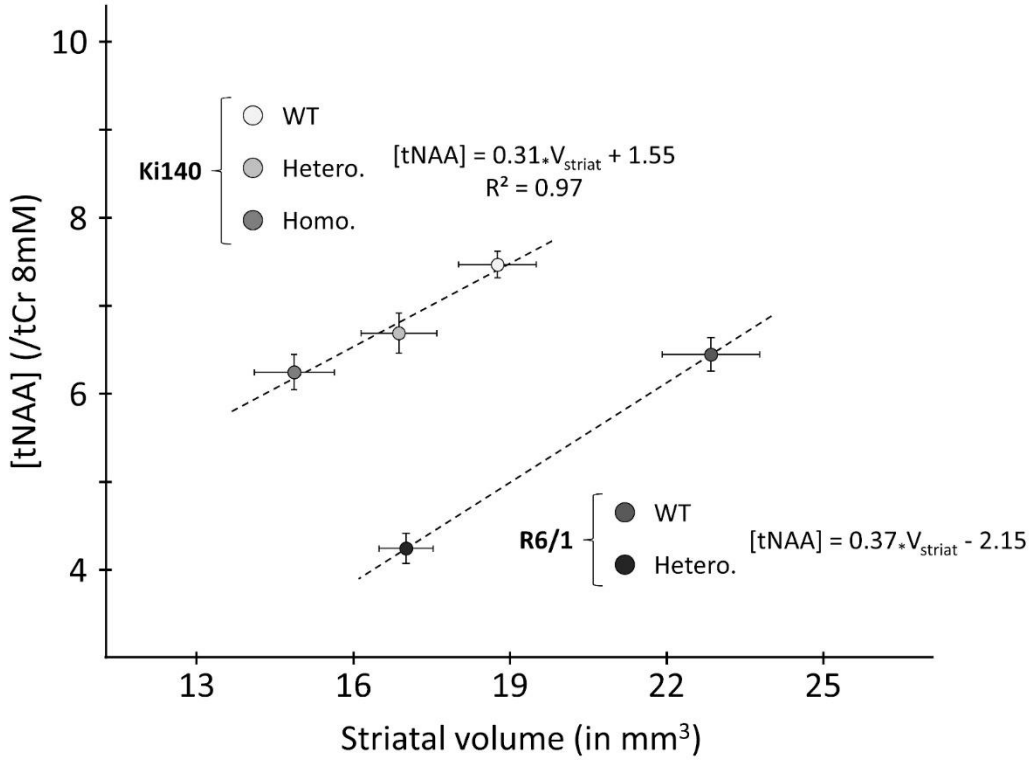

Figure 3: Variation of tNAA concentration as a function of the striatal volume in Ki140CAG and R6/1 mice.

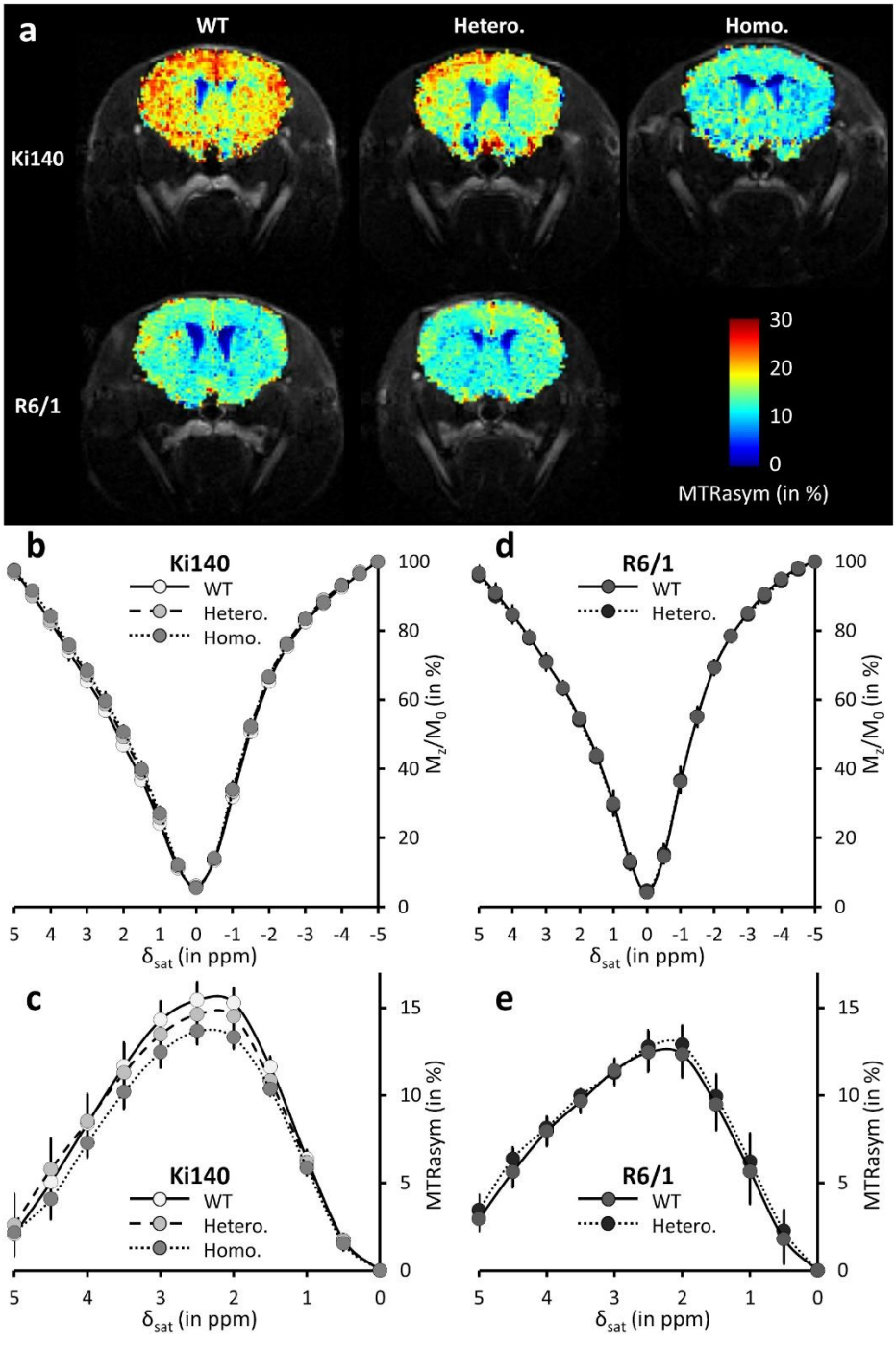

Figure 4: GluCEST imaging in Ki140CAG and R6/1 mice. a) Example of gluCEST images acquired at 3 ppm in Ki140CAG (top panel) and R6/1 (bottom panel) mice in each genotype group (WT littermate control mouse: left panel images; heterozygous mouse: middle panel images; homozygous mouse: right panel images). **b)** Z-spectra acquired in a 2x2x1.8 mm^3 voxel located in the left striatum of WT littermate, heterozygous and homozygous Ki140CAG mice (mean±SEM). **c)** Corresponding MTRasym spectra acquired in Ki140CAG mice. **d)** Z-spectra acquired in a 2x2x1.8 mm^3 voxel located in the left striatum of WT littermate and heterozygous R6/1 mice (mean±SEM). **e)** Corresponding MTRasym spectra acquired in R6/1 mice.

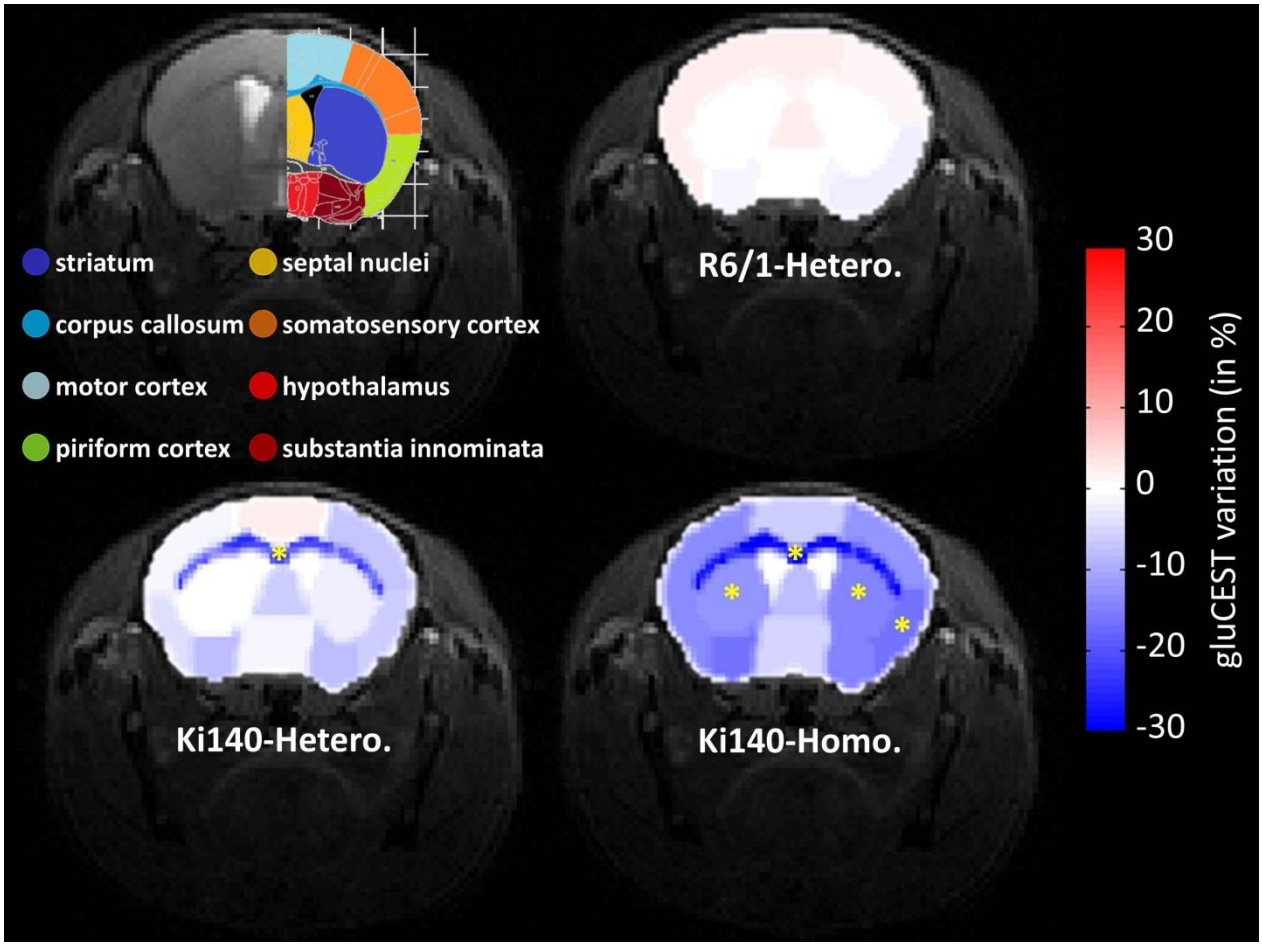

Figure 5: Variation maps of gluCEST contrast in Ki140CAG and R6/1 mice. Mice brain was segmented into 8 ROIs (top left). Variation of gluCEST contrast was calculated in each ROI between WT littermate controls and HD mice as follows: *Variation = 100 x (MTRasym(WT) - MTRasym(HD)) / MTRasym(WT)*. MTRasym(HD) was either mean gluCEST contrast measured in R6/1-Hetero mice (top right), in Ki140-Hetero mice (bottom left) or in Ki140-Homo mice (bottom right). Statistical analysis was performed by Student's t-test for R6/1 mice and by one-way ANOVA (significant threshold set to 0.05) with Fisher's LSD *post hoc* test for Ki140CAG mice (*$p < 0.05$; **$p < 0.01$; ***$p < 0.001$).

References

1. Jellinger KA. Recent advances in our understanding of neurodegeneration. J Neural Transm (Vienna). 2009;116(9):1111-62.
2. Ramanan VK, Saykin AJ. Pathways to neurodegeneration: mechanistic insights from GWAS in Alzheimer's disease, Parkinson's disease, and related disorders. Am J Neurodegener Dis. 2013;2(3):145-75.
3. Aylward EH, Sparks BF, Field KM, Yallapragada V, Shpritz BD, Rosenblatt A, et al. Onset and rate of striatal atrophy in preclinical Huntington disease. Neurology. 2004;63(1):66-72.
4. Tabrizi SJ, Scahill RI, Owen G, Durr A, Leavitt BR, Roos RA, et al. Predictors of phenotypic progression and disease onset in premanifest and early-stage Huntington's disease in the TRACK-HD study: analysis of 36-month observational data. Lancet Neurol. 2013;12(7):637-49.
5. Paulsen JS, Langbehn DR, Stout JC, Aylward E, Ross CA, Nance M, et al. Detection of Huntington's disease decades before diagnosis: the Predict-HD study. J Neurol Neurosurg Psychiatry. 2008;79(8):874-80.
6. DeKosky ST, Marek K. Looking backward to move forward: early detection of neurodegenerative disorders. Science. 2003;302(5646):830-4.
7. Gill SS, Small RK, Thomas DG, Patel P, Porteous R, Van Bruggen N, et al. Brain metabolites as 1H NMR markers of neuronal and glial disorders. NMR Biomed. 1989;2(5-6):196-200.
8. Petroff OA, Pleban L, Prichard JW. Metabolic assessment of a neuron-enriched fraction of rat cerebrum using high-resolution 1H and 13C NMR spectroscopy. Magn Reson Med. 1993;30(5):559-67.
9. Simmons ML, Frondoza CG, Coyle JT. Immunocytochemical localization of N-acetyl-aspartate with monoclonal antibodies. Neuroscience. 1991;45(1):37-45.
10. Brand A, Richter-Landsberg C, Leibfritz D. Multinuclear NMR studies on the energy metabolism of glial and neuronal cells. Dev Neurosci. 1993;15(3-5):289-98.
11. Jenkins BG, Rosas HD, Chen YC, Makabe T, Myers R, MacDonald M, et al. 1H NMR spectroscopy studies of Huntington's disease: correlations with CAG repeat numbers. Neurology. 1998;50(5):1357-65.
12. Schuff N, Meyerhoff DJ, Mueller S, Chao L, Sacrey DT, Laxer K, et al. N-acetylaspartate as a marker of neuronal injury in neurodegenerative disease. Advances in experimental medicine and biology. 2006;576:241-62; discussion 361-3.
13. Tkac I, Dubinsky JM, Keene CD, Gruetter R, Low WC. Neurochemical changes in Huntington R6/2 mouse striatum detected by in vivo 1H NMR spectroscopy. J Neurochem. 2007;100(5):1397-406.
14. Ward KM, Aletras AH, Balaban RS. A new class of contrast agents for MRI based on proton chemical exchange dependent saturation transfer (CEST). Journal of Magnetic Resonance. 2000;143(1):79-87.
15. Wolff S, Balaban R. NMR imaging of labile proton exchange. Journal of Magnetic Resonance. 1990;86:164-9.
16. Cai K, Singh A, Roalf DR, Nanga RP, Haris M, Hariharan H, et al. Mapping glutamate in subcortical brain structures using high-resolution GluCEST MRI. NMR Biomed. 2013;26(10):1278-84.
17. Roalf DR, Nanga RPR, Rupert PE, Hariharan H, Quarmley M, Calkins ME, et al. Glutamate imaging (GluCEST) reveals lower brain GluCEST contrast in patients on the psychosis spectrum. Molecular psychiatry. 2017;22(9):1298-305.
18. Haris M, Nath K, Cai K, Singh A, Crescenzi R, Kogan F, et al. Imaging of glutamate neurotransmitter alterations in Alzheimer's disease. NMR Biomed. 2013;26(4):386-91.
19. Pepin J, Francelle L, Carrillo-de Sauvage MA, de Longprez L, Gipchtein P, Cambon K, et al. In vivo imaging of brain glutamate defects in a knock-in mouse model of Huntington's disease. Neuroimage. 2016;139:53-64.
20. Carrillo-de Sauvage MA, Flament J, Bramoulle Y, Ben Haim L, Guillermier M, Berniard A, et al. The neuroprotective agent CNTF decreases neuronal metabolites in the rat striatum: an in vivo multimodal magnetic resonance imaging study. J Cereb Blood Flow Metab. 2015;35(6):917-21.
21. Farshim PP, Bates GP. Mouse Models of Huntington's Disease. Methods Mol Biol. 2018;1780:97-120.
22. Menalled LB, Sison JD, Dragatsis I, Zeitlin S, Chesselet MF. Time course of early motor and neuropathological anomalies in a knock-in mouse model of Huntington's disease with 140 CAG repeats. The Journal of comparative neurology. 2003;465(1):11-26.

23. Mangiarini L, Sathasivam K, Seller M, Cozens B, Harper A, Hetherington C, et al. Exon 1 of the HD gene with an expanded CAG repeat is sufficient to cause a progressive neurological phenotype in transgenic mice. Cell. 1996;87(3):493-506.
24. Ferrante RJ. Mouse models of Huntington's disease and methodological considerations for therapeutic trials. Biochim Biophys Acta. 2009;1792(6):506-20.
25. Provencher SW. Estimation of metabolite concentrations from localized in vivo proton NMR spectra. Magn Reson Med. 1993;30(6):672-9.
26. Kim M, Gillen J, Landman B, Zhou J, van Zijl P. Water Saturation Shift Referencing (WASSR) for Chemical Exchange Saturation Transfer (CEST) Experiments. Magnetic Resonance in Medicine. 2009;61(6):1441-50.
27. Lerner RP, Trejo Martinez Ldel C, Zhu C, Chesselet MF, Hickey MA. Striatal atrophy and dendritic alterations in a knock-in mouse model of Huntington's disease. Brain research bulletin. 2012;87(6):571-8.
28. Tkac I, Henry PG, Zacharoff L, Wedel M, Gong W, Deelchand DK, et al. Homeostatic adaptations in brain energy metabolism in mouse models of Huntington disease. J Cereb Blood Flow Metab. 2012;32(11):1977-88.
29. Zacharoff L, Tkac I, Song Q, Tang C, Bolan PJ, Mangia S, et al. Cortical metabolites as biomarkers in the R6/2 model of Huntington's disease. J Cereb Blood Flow Metab. 2012;32(3):502-14.
30. Menalled L, El-Khodor BF, Patry M, Suarez-Farinas M, Orenstein SJ, Zahasky B, et al. Systematic behavioral evaluation of Huntington's disease transgenic and knock-in mouse models. Neurobiology of disease. 2009;35(3):319-36.
31. Li JY, Popovic N, Brundin P. The use of the R6 transgenic mouse models of Huntington's disease in attempts to develop novel therapeutic strategies. NeuroRx. 2005;2(3):447-64.
32. Naver B, Stub C, Moller M, Fenger K, Hansen AK, Hasholt L, et al. Molecular and behavioral analysis of the R6/1 Huntington's disease transgenic mouse. Neuroscience. 2003;122(4):1049-57.
33. Langfelder P, Cantle JP, Chatzopoulou D, Wang N, Gao F, Al-Ramahi I, et al. Integrated genomics and proteomics define huntingtin CAG length-dependent networks in mice. Nat Neurosci. 2016;19(4):623-33.
34. Kuhn A, Goldstein DR, Hodges A, Strand AD, Sengstag T, Kooperberg C, et al. Mutant huntingtin's effects on striatal gene expression in mice recapitulate changes observed in human Huntington's disease brain and do not differ with mutant huntingtin length or wild-type huntingtin dosage. Hum Mol Genet. 2007;16(15):1845-61.
35. Hodges A, Strand AD, Aragaki AK, Kuhn A, Sengstag T, Hughes G, et al. Regional and cellular gene expression changes in human Huntington's disease brain. Hum Mol Genet. 2006;15(6):965-77.
36. Galvan L, Francelle L, Gaillard MC, de Longprez L, Carrillo-de Sauvage MA, Liot G, et al. The striatal kinase DCLK3 produces neuroprotection against mutant huntingtin. Brain. 2018;141(5):1434-54.
37. Dautry C, Vaufrey F, Brouillet E, Bizat N, Henry PG, Conde F, et al. Early N-acetylaspartate depletion is a marker of neuronal dysfunction in rats and primates chronically treated with the mitochondrial toxin 3-nitropropionic acid. J Cereb Blood Flow Metab. 2000;20(5):789-99.
38. Choi JK, Dedeoglu A, Jenkins BG. Application of MRS to mouse models of neurodegenerative illness. NMR Biomed. 2007;20(3):216-37.
39. Dubinsky JM. Towards an Understanding of Energy Impairment in Huntington's Disease Brain. J Huntingtons Dis. 2017;6(4):267-302.
40. Cai K, Haris M, Singh A, Kogan F, Greenberg JH, Hariharan H, et al. Magnetic resonance imaging of glutamate. Nat Med. 2012;18(2):302-6.

List of figure legends

Figure 1: Striatal atrophy measured by MRI in Ki140CAG and R6/1 mice. Striatum volume was measured in Ki140-WT (n = 5), Ki140-Hetero. (n = 5), Ki140-Homo. (n = 5), R6/1-WT (n = 3) and R6/1-Hetero (n = 4) mice. Data are presented as mean ± SEM. Statistical analysis was performed by Student's t-test for R6/1 mice and by one-way ANOVA (significant threshold set to 0.05) with Fisher's LSD *post hoc* test for Ki140CAG mice (*$p < 0.05$; **$p < 0.01$; ***$p < 0.001$).

Figure 2: ^{1}H-MRS of Ki140CAG and R6/1 mice. a) Examples of ^{1}H-spectrum acquired in a voxel of 8 µL located in the left striatum (see inset) of one mouse from each group of Ki140CAG mice (top panel) and R6/1 mice (bottom panel). The following metabolites, total choline (*tCho*), total creatine (*tCr*), glutamate (*Glu*), glutamine (*Gln*), myo-inositol (*Ins*), total N-acetyl-aspartate + N-acetyl-aspartyl-glutamate (*tNAA*) and taurine (*Tau*), were reliably quantified (CRLB < 5%). **b)** Metabolic profiles measured by ^{1}H-MRS in Ki140CAG and R6/1 mice. Concentration of metabolites normalized with respect to 8 mM tCr were measured in left striatum of Ki140-WT (n = 5), Ki140-Hetero. (n = 5), Ki140-Homo. (n = 5), R6/1-WT (n = 3) and R6/1-Hetero (n = 4) mice. Data are presented as mean ± SEM. Statistical analysis was performed by Student's t-test for R6/1 mice and by one-way ANOVA (significant threshold set to 0.05) with Fisher's LSD *post hoc* test for Ki140CAG mice (*$p < 0.05$; **$p < 0.01$; ***$p < 0.001$).

Figure 3: Variation of tNAA concentration as a function of the striatal volume in Ki140CAG and R6/1 mice.

Figure 4: GluCEST imaging in Ki140CAG and R6/1 mice. a) Example of gluCEST images acquired at 3 ppm in Ki140CAG (top panel) and R6/1 (bottom panel) mice in each genotype group (WT littermate control mouse: left panel images; heterozygous mouse: middle panel images; homozygous mouse: right panel images). **b)** Z-spectra acquired in a 2x2x1.8 mm^3 voxel located in the left striatum of WT littermate, heterozygous and homozygous Ki140CAG mice (mean±SEM). **c)** Corresponding MTRasym spectra acquired in Ki140CAG mice. **d)** Z-spectra acquired in a 2x2x1.8 mm^3 voxel located in the left striatum of WT littermate and heterozygous R6/1 mice (mean±SEM). **e)** Corresponding MTRasym spectra acquired in R6/1 mice.

Figure 5: Variation maps of gluCEST contrasts in Ki140CAG and R6/1 mice. Mice brain was segmented into 8 ROIs (top left). Variation of gluCEST contrast was calculated in each ROI between WT littermate controls and HD mice as follows: *Variation = 100 x (MTRasym(WT) - MTRasym(HD)) / MTRasym(WT)*. MTRasym(HD) was either mean gluCEST contrast measured in R6/1-Hetero mice (top right), in Ki140-Hetero mice (bottom left) or in Ki140-Homo mice (bottom right). Statistical analysis was performed by Student's t-test for R6/1 mice and by one-way ANOVA (significant threshold set to 0.05) with Fisher's LSD *post hoc* test for Ki140CAG mice (*$p < 0.05$; **$p < 0.01$; ***$p < 0.001$).

List of Abbreviations

CEST: Chemical Exchange Saturation Transfer
DARPP-32: 3′,5′-Cyclic Adenosine Monophosphate-Regulated Neuronal Phosphoprotein
DCLK3: doublecortin-like kinase 3
GABA: gamma-Aminobutyric acid
Gln: Glutamine
Glu: Glutamate
gluCEST: CEST imaging of glutamate
HD: Huntington's disease
Hetero: Heterozygous
Homo: Homozygous
Htt: Murine huntingtin gene
HTT: Human huntingtin gene
Ins: Myo-inositol
LASER: Localization by Adiabatic Selective Refocusing
MSME: Multi Slices Multi Echoes
MTRasym: Asymmetrical Magnetization Transfer Ratio
NAA: N-acetylaspartate
PDE10: phosphodiesterase 10
ROIs: Regions-of-interest
Tau: Taurine
tCho: Total choline
tCr: Total creatine
tNAA: total N-acetyl-aspartate + N-acetyl-aspartyl-glutamate
VAPOR: Variable power radiofrequency pulses with optimized relaxation delays
WASSR: Water Saturation Shift Referencing
WT: Wild type